UDC 539.14

GIANT RESONANCES UNDER EXTREME CONDITIONS

N. Dinh Dang[1,2]

[1]*Heavy-ion nuclear physics laboratory, Nishina Center for Accelerator-Based Science, Hirosawa, Wako city, Saitama, Japan*
[2]*Institute for Nuclear Science and Technique, Hanoi, Vietnam*

The theoretical description of nuclear resonances at zero and finite temperatures is presented. The following issues are addressed: 1) Giant dipole resonances (GDR) in highly excited nuclei, including both low and high regions of temperature. The results of calculations are obtained within the phonon-damping model, thermal shape-fluctuation model including thermal pairing, and compared with experimental data. 2) The electromagnetic cross sections of the double GDRs (DGDR) in ^{136}Xe and ^{208}Pb. The results obtained in theoretical calculations are compared with the experimental data for the DGDR cross sections in exclusive measurements at near-relativistic energies. 3) GDR and pygmy dipole resonances (PDR) in neutron-rich nuclei, where the effect of coupling of the GDR to complicated configurations on the PDR is analyzed.

1. Introduction

Nuclear resonances under extreme conditions mentioned in the present lecture include i) giant dipole resonances (GDR) in highly excited nuclei formed in heavy-ion reactions and inelastic scattering of light particles or nuclei on heavy targets, ii) double GDRs (DGDR) formed in Coulomb excitations at near relativistic energies, and iii) pygmy dipole resonances (PDR) in neutron-rich nuclei.

The recent studies of these resonances have been facing the following challenges:

1. The GDR has been observed in highly-excited (hot) nuclei. These nuclei are formed as compound nuclei at high excitation energies E^* in heavy-ion fusion reactions or in the inelastic scattering of light particles (nuclei) on a heavy nucleus. The γ-decay spectra of these compound nuclei show the existence of the GDR, whose peak energy depends weakly on the excitation energy E^*. The dependence of the GDR on the temperature T has been experimentally extracted when the angular momentum of the compound nucleus is low, as in the case of the light-particle scattering experiments, or when it can be separated out from the excitation energy E^*. It has been experimentally found that the GDR's full width at the half maximum (FWHM) remains almost constant at $T \leq$ 1 MeV, but sharply increases with T up to $T \simeq$ 2 - 3 MeV, and saturates at higher T [1].

2. The DGDR has been observed in the Coulomb excitations of ^{136}Xe and ^{208}Pb projectiles on ^{208}Pb target at the bombarding energies of 0.7 GeV/n and 0.64 GeV/n, respectively. The extracted electromagnetic (EM) cross sections of the DGDR in these experiments have been compared with theoretical predictions based on the non-interacting phonon (harmonic) picture. The latter calculates the parameters of the DGDR by folding to independent GDRs. As a result, the DGDR energy $E_{\rm DGDR}$ is found to be equal to $2E_{\rm GDR}$ ($E_{\rm GDR}$ is the GDR energy), and the DGDR FWHM $\Gamma_{\rm DGDR}$ is equal to $2\Gamma_{\rm GDR}$ ($\Gamma_{\rm GDR}$ is the GDR FWHM) if Lorentzian photoabsorption cross sections are used in folding the GDRs, or to $\sqrt{2}\Gamma_{\rm GDR}$, if Gaussians are folded. The comparison shows that the experimentally extracted energy and width of DGDR differ slightly from these values. The most striking discrepancy is that the experimental EM cross sections are much larger that than the values predicted by the folding model. The enhancement is found to be around 178 % for ^{136}Xe and 133 % for ^{208}Pb [3].

3. It is well believed that, in neutron-rich nuclei, the oscillation of the neutron excess against the stable core may cause a low-frequency E1 resonance, which is called the pygmy dipole resonance (PDR). However, in the case when the neutron excess cannot be well separated from the stable core, the coupling between them may lead to a strong fragmentation of the PDR. As a result the pygmy dipole mode may become non-collective. Theoretical calculations within the relativistic RPA and the particle-hole $(ph)\oplus$phonon-coupling model so far have given contradicting predictions. The former shows a clear PDR bump with a peak at around 8 MeV, while no evidence for collectivity is seen below 10 MeV in the latter [3].

It will be shown in the present lecture how the above-mentioned issues are interpreted within the phonon-damping model (PDM) [4]. The PDM was originally proposed in 1998 with the primary aim to describe the damping of the hot GDR. This model was extended later to address the issue of anharmonicity in the DGDR. By including pairing, the model is also able to predict the GDR's width at low T as well as the EM cross sections of E1 excitations in neutron-rich nuclei.

2. Outline of the PDM

A. Damping of hot GDR

The quasiparticle representation of the PDM Hamiltonian [5] is obtained by adding the superfluid pairing interaction and expressing the particle (p) and hole (h) creation and destruction operators, $a_s^\dagger$ and a_s ($s = p,h$), in terms of the quasiparticle operators, $\alpha_s^\dagger$ and α_s, using the Bogolyubov's canonical transformation. As a result, the PDM Hamiltonian for the description of Eλ excitations can be written in spherical basis as

$$H = \sum_{jm} E_j \alpha_{jm}^\dagger \alpha_{jm} + \sum_{\lambda\mu i} \omega_{\lambda i} b_{\lambda\mu i}^\dagger b_{\lambda\mu i} + \\ + \frac{1}{2} \sum_{\lambda\mu i} \frac{(-)^{\lambda-\mu}}{\hat{\lambda}} \sum_{jj'} f_{jj'}^{(\lambda)} \{ u_{jj'}^{(+)} [A_{jj'}^\dagger(\lambda\mu) + A_{jj'}(\lambda\tilde{\mu})] + v_{jj'}^{(-)} [B_{jj'}^\dagger(\lambda\mu) + B_{jj'}(\lambda\tilde{\mu})] \} (b_{\lambda\mu i}^\dagger + b_{\lambda\tilde{\mu} i}) , \tag{1}$$

where $\hat{\lambda} = \sqrt{2\lambda+1}$. The first term at the right-hand side (rhs) of Hamiltonian (1) corresponds to the independent-quasiparticle field. The second term stands for the phonon field described by phonon operators, $b_{\lambda\mu i}^\dagger$ and $b_{\lambda\mu i}$, with multipolarity λ, which generate the harmonic collective vibrations such as GDR. Phonons are ideal bosons within the PDM, i.e. they have no fermion structure. The last term is the coupling between quasiparticle and phonon fields, which is responsible for the microscopic damping of collective excitations.

In Eq. (1) the following standard notations are used

$$A_{jj'}^\dagger(\lambda\mu) = \sum_{mm'} \langle jmj'm' \mid \lambda\mu \rangle \alpha_{jm}^\dagger \alpha_{j'm'}^\dagger , B_{jj'}^\dagger(\lambda\mu) = -\sum_{mm'} (-)^{j'-m'} \langle jmj'-m' \mid \lambda\mu \rangle \alpha_{jm}^\dagger \alpha_{j'm'} , \tag{2}$$

with $(\lambda\tilde{\mu}) \longleftrightarrow (-)^{\lambda-\mu}(\lambda-\mu)$. Functions $u_{jj'}^{(+)} \equiv u_j v_{j'} + v_j u_{j'}$ and $v_{jj'}^{(-)} \equiv u_j u_{j'} - v_j v_{j'}$ are combinations of Bogolyubov's u and v coefficients. The quasiparticle energy E_j is calculated from the single-particle energy ε_j as

$$E_j = \sqrt{(\varepsilon_j - \varepsilon_{\mathrm{F}})^2 + \Delta^2} , \varepsilon_j \equiv \varepsilon_j - G v_j^2, \tag{3}$$

where the pairing gap Δ and the Fermi energy ε_{F} are defined as solutions of the BCS equations. At $T \neq 0$ the thermal pairing gap $\Delta(T)$ (or $\overline{\Delta}(T)$) is defined from the finite-temperature BCS (or modified BCS) equations (See section C below).

The equation for the propagation of the GDR phonon, which is damped due to coupling to the quasiparticle field, is derived making use of the double-time Green's function method (introduced by Bogolyubov and Tyablikov, and developed further by Zubarev). Following the standard procedure of deriving the equation for the double-time retarded Green's function with respect to the Hamiltonian (1); one obtains a closed set of equations for the Green's functions for phonon and quasiparticle propagators. Making the Fourier transform into the energy plane E, and expressing all the Green functions in the set in terms of the one-phonon propagation Green function, we obtain the equation for the latter, $G_{\lambda i}(E)$, in the form

$$G_{\lambda i}(E) = \frac{1}{2\pi} \frac{1}{E - \omega_{\lambda i} - P_{\lambda i}(E)} , \tag{4}$$

where the explicit form of the polarization operator $P_{\lambda i}(E)$ is

$$P_{\lambda i}(E) = \frac{1}{\hat{\lambda}^2} \sum_{jj'} [f_{jj'}^{(\lambda)}]^2 \left[\frac{(u_{jj'}^{(+)})^2 (1 - n_j - n_{j'})(\varepsilon_j + \varepsilon_{j'})}{E^2 - (\varepsilon_j + \varepsilon_{j'})^2} - \frac{(v_{jj'}^{(-)})^2 (n_j - n_{j'})(\varepsilon_j - \varepsilon_{j'})}{E^2 - (\varepsilon_j - \varepsilon_{j'})^2} \right] . \tag{5}$$

The polarization operator (5) appears due to ph – phonon coupling in the last term of the rhs of Hamiltonian (1). The phonon damping $\gamma_{\lambda i}(\omega)$ (ω real) is obtained as the imaginary part of the analytic

continuation of the polarization operator $P_{\lambda i}(E)$ into the complex energy plane $E = \omega \pm i\varepsilon$. Its final form is

$$\gamma_{\lambda i}(\omega) = \frac{\pi}{2\hat{\lambda}^2}\sum_{jj'}[f_{jj'}^{(\lambda)}]^2\{(u_{jj'}^{(+)})^2(1-n_j-n_{j'})[\delta(E-E_j-E_{j'})-\delta(E+E_j+E_{j'})]- \\ (v_{jj'}^{(-)})^2(n_j-n_{j'})[\delta(E-E_j+E_{j'})-\delta(E+\varepsilon_j-\varepsilon_{j'})]\}. \tag{6}$$

The quasiparticle occupation number n_j is calculated as

$$n_j = \frac{1}{\pi}\int_{-\infty}^{\infty}\frac{n_{\mathrm{F}}(E)\gamma_j(E)}{[E-E_j-M_j(E)]^2+\gamma_j^2(E)}dE\,, n_{\mathrm{F}}(E) = (\mathrm{e}^{E/T}+1)^{-1}\,, \tag{7}$$

where $M_j(E)$ is the mass operator, and $\gamma_j(E)$ is the quasiparticle damping, which is determined as the imaginary part of the complex continuation of $M_j(E)$ into the complex energy plane [5]. These quantities appear due to coupling between quasiparticles and the GDR. From Eq. (7) it is seen that the functional form for the occupation number n_j is not given by the Fermi-Dirac distribution $n_{\mathrm{F}}(E_j)$ for non-interacting quasiparticles. It can be approximately to be so if the quasiparticle damping $\gamma_j(E)$ is sufficiently small. Equation (7) also implies a zero value for n_j in the ground state, i.e. $n_j(T=0) = 0$. In general, it is not the case because of ground-state correlations beyond the quasiparticle RPA (QRPA). They lead to $n_j(T=0) \neq 0$, which should be found by solving self-consistently a set of nonlinear equations within the renormalized QRPA. However, for collective high-lying excitations such as GDR, the value $n_j(T=0)$ is negligible.

The energy $\bar{\omega}$ of giant resonance (damped collective phonon) is found as the solution of the equation: $\bar{\omega} - \omega_{\lambda i} - P_{\lambda i}(\bar{\omega}) = 0$. The width Γ_λ of giant resonance is calculated as twice of the damping $\gamma_\lambda(\omega)$ at $\omega = \bar{\omega}$, where $\lambda = 1$ corresponds to the GDR width Γ_{GDR}. The latter is conveniently decomposed into the quantal (Γ_{Q}) and thermal (Γ_{T}) widths as

$$\Gamma_{\mathrm{GDR}} = \Gamma_{\mathrm{Q}} + \Gamma_{\mathrm{T}}\,, \tag{8a}$$

$$\Gamma_{\mathrm{Q}} = 2\pi F_1^2\sum_{ph}[u_{ph}^{(+)}]^2(1-n_p-n_h)\delta(E_{\mathrm{GDR}}-E_p-E_h)\,, \tag{8b}$$

$$\Gamma_{\mathrm{T}} = 2\pi F_2^2\sum_{s>s'}[v_{ss'}^{(-)}]^2(n_{s'}-n_s)\delta(E_{\mathrm{GDR}}-E_s+E_{s'})\,, \tag{8c}$$

where $(ss') = (pp')$ and (hh') with p and h denoting the orbital angular momenta j_p and j_h for particles and holes, respectively. The quantal and thermal widths come from the couplings of quasiparticle pairs $[\alpha_p^\dagger \otimes \alpha_h^\dagger]_{LM}$ and $[\alpha_s^\dagger \otimes \alpha_{\tilde{s}'}]_{LM}$ to the GDR, respectively. At zero pairing they correspond to the couplings of ph pairs, $[a_p^\dagger \otimes a_{\tilde{h}}]_{LM}$, and pp (hh) pairs, $[a_s^\dagger \otimes a_{\tilde{s}'}]_{LM}$, to the GDR, respectively (the tilde ~ denotes the time-reversal operation).

The line shape of the GDR is described by the strength function $S_{\mathrm{GDR}}(\omega)$, which is derived from the spectral intensity in the standard way using the analytic continuation of the Green function (4) and by expanding the polarization operator (5) around $\omega = E_{\mathrm{GDR}}$. The final form of $S_{\mathrm{GDR}}(\omega)$ is [4, 5]

$$S_{\mathrm{GDR}}(\omega) = \frac{1}{\pi}\frac{\gamma_{\mathrm{GDR}}(\omega)}{(\omega-E_{\mathrm{GDR}})^2+\gamma_{\mathrm{GDR}}^2(\omega)}\,. \tag{9}$$

The photoabsorption cross section $\sigma(E_\gamma)$ is calculated from the strength function $S_{\mathrm{GDR}}(E_\gamma)$ as

$$\sigma(E_\gamma) = c_1 S_{\mathrm{GDR}}(E_\gamma)E_\gamma\,, \tag{10}$$

where $E_\gamma \equiv \omega$ is used to denote the energy of γ-emission. The normalization factor c_1 is defined so that the total integrated photoabsorption cross section $\sigma = \int \sigma(E_\gamma) dE_\gamma$ satisfies the GDR sum rule $\mathrm{SR_{GDR}}$, hence

$$c_1 = \mathrm{SR_{GDR}} \Big/ \int_0^{E_{\max}} S_{\mathrm{GDR}}(E_\gamma) E_\gamma dE_\gamma \,. \tag{11}$$

In heavy nuclei with $A \geq$ 40, the GDR exhausts the Thomas-Reich-Kuhn sum rule (TRK) $\mathrm{SR_{GDR}} = \mathrm{TRK} \equiv 60\ NZ/A$ (MeV · mb) at the upper integration limit $E_{\max} \simeq$ 30 MeV, and exceeds TRK ($\mathrm{SR_{GDR}} > \mathrm{TRK}$) at $E_{\max} >$ 30 MeV due to the contribution of exchange forces. In some light nuclei, such as ^{16}O, the observed photoabsorption cross section exhausts only around 60 % of TRK up to $E_{\max} \simeq$ 30 MeV.

B. Thermal pairing

The standard finite-temperature BCS (FT-BCS) theory ignores fluctuations of the quasiparticle number. As a result, the BCS breaks down at a critical temperature $T_c \simeq 0.567\Delta(T=0)$, which corresponds to the sharp transition from the superfluid phase to the normal-fluid one. It has been known that, in finite systems such as nuclei, thermal fluctuations smooth out this phase transition [6].

The modified BCS (MBCS) theory [7] proposes a microscopic way to include quasiparticle-number fluctuations via the secondary Bogolyubov's transformation

$$\bar{\alpha}^\dagger_{jm} = \sqrt{1-n_j}\,\alpha^\dagger_{jm} + \sqrt{n_j}\,\alpha_{j\tilde{m}}\,, \bar{\alpha}_{j\tilde{m}} = \sqrt{n_j}\,\alpha_{j\tilde{m}} - \sqrt{n_j}\,\alpha^\dagger_{jm}\,. \tag{12}$$

Using Eqs. (12) in combination with the original Bogolyubov's transformation, one obtains the transformation from the particle operators directly to the modified quasiparticle operators in the following form

$$a^\dagger_{jm} = \bar{u}_j \bar{\alpha}^\dagger_{jm} + \bar{v}_j \bar{\alpha}_{j\tilde{m}}\,, a_{j\tilde{m}} = \bar{u}_j \bar{\alpha}_{j\tilde{m}} - \bar{v}_j \bar{\alpha}^\dagger_{jm}\,, \tag{13}$$

where the coefficients $\bar{u}_j$ and $\bar{v}_j$ are related to the conventional Bogolyubov's coefficients u_j and v_j as

$$\bar{u}_j = u_j\sqrt{1-n_j} + v_j\sqrt{n_j}\,, \bar{v}_j = v_j\sqrt{1-n_j} - u_j\sqrt{n_j}\,. \tag{14}$$

The transformation of the pairing Hamiltonian (1) into the modified quasiparticles $\bar{\alpha}^\dagger_{jm}$ and $\bar{\alpha}_{jm}$ has the form identical to that obtained within the conventional quasiparticle representation with ($\bar{u}_j$, $\bar{v}_j$) replacing (u_j, v_j) and ($\bar{\alpha}^\dagger_{jm}$, $\bar{\alpha}_{jm}$) replacing ($\alpha^\dagger_{jm}$, α_{jm}), respectively. The MBCS equations, therefore, has exactly the same form as that of the standard BCS equations, where the coefficients u_j and v_j are replaced with $\bar{u}_j$ and $\bar{v}_j$, i.e.

$$\bar{\Delta} = G\sum_j \Omega_j \bar{u}_j \bar{v}_j = G\sum_j \Omega_j[(1-2n_j)u_j v_j - \sqrt{n_j(1-n_j)}(u_j^2 - v_j^2)]\,, \tag{15}$$

$$N = 2\sum_j \Omega_j \bar{v}_j^2 = 2\sum_j \Omega_j[(1-2n_j)v_j^2 + n_j - 2\sqrt{n_j(1-n_j)}u_j v_j]\,, \tag{16}$$

The last terms at the rhs of these MBCS equations contain the quasiparticle-number fluctuations $\sqrt{n_j(1-n_j)}$ on $j-$th orbitals, which are not included in the standard FT-BCS theory.

C. EM cross sections of GDR and DGDR

The EM cross section σ_{EM} is calculated from the corresponding photoabsorption cross section $\sigma(E_\gamma)$ and the photon spectral function $N(E_\gamma)$ as

$$\sigma_{\mathrm{EM}} = \int N(E_\gamma)\sigma(E_\gamma)dE_\gamma, N(E_\gamma) = 2\pi\int_{b_{\min}}^{\infty} \mathrm{e}^{-m(b)} N(E_\gamma, b) b db. \tag{17}$$

The expression for the spectrum $N(E_\gamma,b)$ of virtual photons from a stationary target as seen by a projectile moving with a velocity $\beta = v/c$ at the impact parameter b is also given in [8]. The average number of photons absorbed by the projectile is calculated as $m(b) = \int_{E_{\min}}^{\infty} N(E_\gamma,b)\sigma(E_\gamma)dE_\gamma$.

The DGDR strength function is calculated within the PDM as

$$S_{\mathrm{DGDR}}^{\mathrm{PDM}}(E) = \frac{2}{\pi}\frac{\gamma_{\mathrm{DGDR}}(E)}{(E-E_{\mathrm{DGDR}})^2+[\gamma_{\mathrm{DGDR}}(E)]^2}, \tag{18}$$

where the DGDR energy E_{DGDR} and damping $\gamma_{\mathrm{DGDR}}(E)$ are calculated microscopically within the PDM (See details in Ref. [9]). The DGDR cross section $\sigma_{\mathrm{DGDR}}(E)$ is calculated as

$$\sigma_{\mathrm{DGDR}}(E) = c^{(2)} S_{\mathrm{DGDR}}^{\mathrm{PDM}}(E)E\,. \tag{19}$$

The DGDR strength factor $c^{(2)}$ in (19) as follows. Using (17) and the harmonic limit $S_{\mathrm{DGDR(har)}}^{\mathrm{PDM}}(E)$ of the DGDR strength function (20), which is obtained by folding two GDR strength functions (9) (pairing not included), we write the formal expression of the harmonic limit $\sigma_{\mathrm{C}}^{(2)}(\mathrm{har})$ of the EM cross section (17) for DGDR as

$$\sigma_{\mathrm{C}}^{(2)}(\mathrm{har}) = \int \frac{d\sigma_{\mathrm{C}}^{(2)}}{dE}(\mathrm{har})dE = c^{(2)}\int N_{\mathrm{har}}(E)S_{\mathrm{DGDR(har)}}^{\mathrm{PDM}}(E)EdE, \tag{20}$$

where $N_{\mathrm{har}}(E)$ is calculated using the harmonic limit $\sigma_{\mathrm{DGDR(har)}}^{PDM}(E)$ of (19) in (17) and $m(b)$. We require this cross section (20) to be equal to the one calculated by folding two GDR cross sections, namely

$$\sigma_{\mathrm{C(f)}}^{(2)} \equiv \int \frac{d\sigma_{\mathrm{C(f)}}^{(2)}}{dE}dE = \frac{1}{2}\int dEdE_1dE_2N(E_1,E_2)\sigma_{\mathrm{GDR}}(E_1)\sigma_{\mathrm{GDR}}(E_2)\delta(E-E_1-E_2) =$$

$$\frac{[c^{(1)}]^2}{\pi}\int dEdE_1dE_2N(E_1,E_2)S_{\mathrm{GDR}}^{\mathrm{PDM}}(E_1)S_{\mathrm{GDR}}^{\mathrm{PDM}}(E_2)E_1E_2\varepsilon/[(E-E_1-E_2)^2+\varepsilon^2], \tag{21}$$

where the representation $\delta(x) = [(x-i\varepsilon)^{-1}-(x+i\varepsilon)^{-1}]/(2\pi i)$ and the expression for $N(E_1,E_2)$ given in [8] are used. Equalizing the right-hand sides of (20) and (21), we define $c^{(2)}$. Knowing $c^{(2)}$, we can calculate the EM cross section $\sigma_{\mathrm{C}}^{(2)}$ of the DGDR from (20) using $S_{\mathrm{DGDR}}^{\mathrm{PDM}}(E)$ (18) instead of its harmonic limit.

3. Numerical results

A. Assumptions and parameters of PDM

The PDM is based on the following assumptions:

a1) The matrix elements for the coupling of GDR to non-collective ph configurations, which causes the quantal width Γ_{Q} (9), are all equal to F_1. Those for the coupling of GDR to pp (hh), which causes the thermal width Γ_{T} (10), are all equal to F_2.

a2) It is well established that the microscopic mechanism of the quantal (spreading) width Γ_{Q} (9) comes from quantal coupling of ph configurations to more complicated ones, such as $2p2h$ ones. The calculations performed in Refs. [10] within two independent microscopic models, where such couplings to $2p2h$ configurations were explicitly included, have shown that Γ_{Q} depends weakly on T. Therefore, in order to avoid complicate numerical calculations, which are not essential for the increase of Γ_{GDR} at $T \neq 0$, such microscopic mechanism is not included within PDM, assuming that Γ_{Q} at $T = 0$ is known. The model parameters are then chosen so that the calculated Γ_{Q} and E_{GDR} reproduce the corresponding experimental values at $T = 0$.

Within assumptions (a1) and (a2) the model has only three T-independent parameters, which are the unperturbed phonon energy ω_q, F_1, and F_2. The parameters ω_q and F_1 are chosen so that after the ph-GDR coupling is switched on, the calculated GDR energy E_{GDR} and width Γ_{GDR} reproduce the corresponding experimental values for GDR on the ground-state. At $T \neq 0$, the coupling to pp and hh configurations is activated. The F_2 parameter is then fixed at $T = 0$ so that the GDR energy E_{GDR} does not change appreciably with T.

B. Temperature dependence of GDR width

Shown in Fig. 1, *a* is the T dependence of the neutron pairing gap $\overline{\Delta}_\nu$ for ^{120}Sn, which is obtained from the MBCS equation (15) using the single-particle energies determined within the Woods - Saxon potential at $T = 0$. The pairing parameter G_ν is chosen to be equal to 0.13 MeV, which yields $\overline{\Delta}(T=0) \equiv \overline{\Delta}(0) \simeq 1.4$ MeV. Contrary to the BCS gap (dotted line), which collapses at $T_{\mathrm{c}} \simeq 0.79$ MeV, the gap $\overline{\Delta}$ (solid line) does not vanish, but decreases monotonously with increasing T at T 1 MeV resulting in a long tail up to $T \simeq 5$ MeV. This behavior is caused by the thermal fluctuation of quasiparticle number in the MBCS equations (15) and (16).

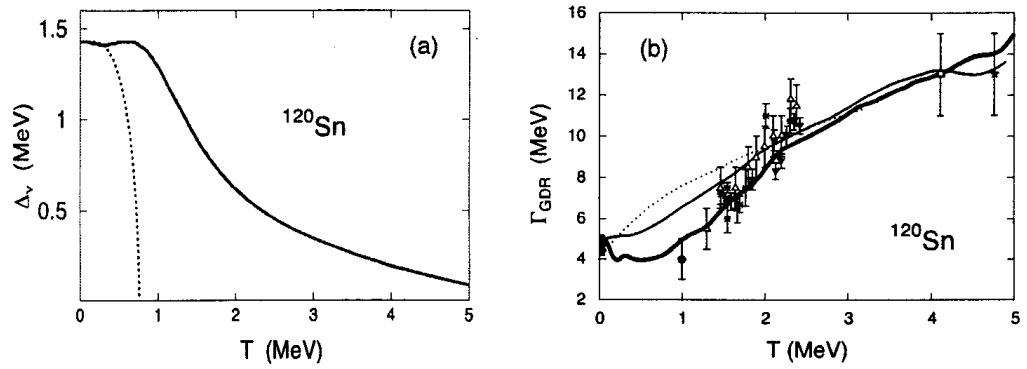

Fig. 1. Neutron pairing gap for ^{120}Sn as a function of T. Solid and dotted lines show the MBCS and BCS gaps, respectively (*a*). GDR width Γ_{GDR} as a function of T for ^{120}Sn (*b*). The thin and thick solid lines show the PDM results obtained neglecting pairing and including the renormalized gap $\widetilde{\Delta} = [1 + 1/\delta N^2]\overline{\Delta}$, respectively. The gap $\widetilde{\Delta}$ includes the correction $\delta N^2 = \overline{\Delta}(0)^2 \sum_j (j+1/2)/[(\varepsilon_j - \overline{\varepsilon}_{\mathrm{F}})^2 + \overline{\Delta}(0)^2]$ due to an approximate number projection. The prediction by the TFM is shown as the dotted line [11].

The GDR widths as a function of T for ^{120}Sn obtained within the PDM are compared in Fig. 1, *b* with the experimental data and the prediction by the thermal fluctuation model (TFM) [11]. The TFM interprets the broadening of the GDR's width via an adiabatic coupling of GDR to quadrupole deformations induced by thermal fluctuations. Even when thermal pairing is neglected the PDM prediction, (the thin solid line) is already better than that given by the TFM, including the region of high T where the width's saturation is reported. The increase of the total width with T is driven by the increase of the thermal width Γ_{T} (8c), which is caused by coupling to pp and hh configurations, since the quantal width Γ_{Q} (8b) is found to decrease slightly with increasing T. The inclusion of thermal pairing, which yields a sharper Fermi surface, compensates the smoothing of the Fermi surface with increasing T. This leads to a much weaker T-dependence of the GDR's width at low T. As a result, the values of the width predicted by the PDM in this region significantly drop (the thick solid line), recovering the data point at $T = 1$ MeV.

The results discussed above have also been confirmed by our recent calculations within a macroscopic approach, which takes pairing fluctuations into account along with the thermal shape fluctuations [12]. Here the free energies are calculated using the Nilsson - Strutinsky method at $T \neq 0$, including thermal pairing correlations. The GDR is coupled to the nuclear shapes through a simple anisotropic harmonic oscillator model with a separable dipole-dipole interaction. The observables are averaged over the shape parameters and pairing gap. Our study reveals that the observed quenching of GDR width at low T in ^{120}Sn and ^{148}Au can be understood in terms of simple shape effects caused by pairing correlations. Fluctuations in pairing field lead to a slowly vanishing pairing gap (Fig. 2, *a*), which influences the structural properties even at moderate T (~ 1 MeV). We found that the low T-structure and hence the GDR width are quite sensitive to the change of the pairing field (Fig. 2, *b*).

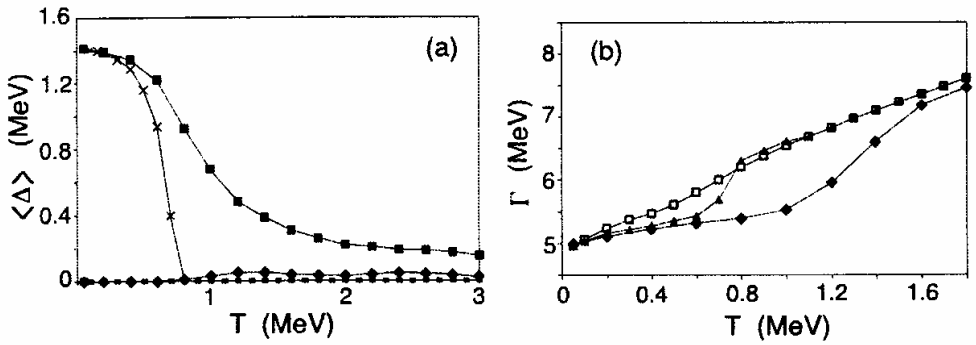

Fig. 2. Pairing gaps for ^{120}Sn averaged over thermal shape fluctuations versus T. Lines with triangles and crosses are the usual BCS proton and neutron pairing gaps, respectively, while those with diamonds and squares denote the corresponding pairing gaps, which also include thermal fluctuations of pairing fields (*a*). GDR widths for ^{120}Sn versus T (*b*). Open squares, triangles, and diamonds denote the widths obtained without pairing, including BCS pairing, and thermally fluctuating pairing field from (*a*), respectively.

C. EM cross section of DGDR

The calculations employ the single-particle energies for ^{136}Xe and ^{208}Pb obtained within the Hartree - Fock (HF) method using the SGII interaction. The unperturbed phonon energy ω_q and the degenerate ph matrix element F_{ph} are chosen so that the GDR energy E_{GDR} and FWHM Γ_{GDR}, obtained within the PDM, reproduce the experimentally extracted values.

The peak energies E_{i}, FWHM Γ_{i}, and EM cross section $\sigma_{\mathrm{C}}^{\mathrm{i}}$ for GDR (i = GDR) and DGDR (i = DGDR) predicted by the PDM are shown in Table in comparison with the experimental data for ^{136}Xe and ^{208}Pb [3]. It is seen that all the calculated values are in reasonable agreement with the corresponding experimental values. K. Boretzky of the LAN collaboration has folded the PDM strength functions for GDR and DGDR with the detector response and plotted the obtained results against the experimental fits in Fig. 3, which shows a remarkable agreement between the PDM predictions and the experimental data.

The energies E_{i}, FWHM Γ_{i}, and EM cross section $\sigma_{\mathrm{C}}^{\mathrm{i}}$ for GDR (i = GDR) (a) and DGDR (i = DGDR) (b), calculated within PDM (Theory) in comparison with the experimental data (Experiment) for ^{136}Xe and ^{208}Pb

a	E_{GDR}, MeV		Γ_{GDR}, MeV		$\sigma_{\mathrm{C}}^{\mathrm{GDR}}$, mb	
Nucleus	Theory	Experiment	Theory	Experiment	Theory	Experiment
^{136}Xe	15.6	15.2	4.96	4.8	1676.28	1420(42) ± 100
^{208}Pb	13.5	13.4	4.04	4.0	3039.67	3280 ± 50
b	E_{DGDR}, MeV		Γ_{DGDR}, MeV		$\sigma_{\mathrm{C}}^{\mathrm{DGDR}}$, mb	
Nucleus	Theory	Experiment	Theory	Experiment	Theory	Experiment
^{136}Xe	29.2	28.3 ± 0.7	7.0	6.3 ± 1.6	159.33	164(85) ± 35
^{208}Pb	26.6	26.6 ± 0.8	6.3	6.3 ± 1.3	420.92	380 ± 40

D. E1-excitations in neutron-rich nuclei

The calculations of photoabsorption and EM cross sections have been carried out for oxygen isotopes with A = 16, 18, 20, 22, and 24, and for calcium isotopes with A = 40, 42, 44, 46, 48, 50, 52, and 60. The calculations employ the spherical-basis single-particle energies E_j obtained within the HF method using the SGII interaction. The two PDM parameters ω_λ (λ = 1) and $F_1 = f_{jj'}^{(1)}$ for all ph indices ($j = p, j' = h$) are chosen in such a way that the values of GDR energy E_{GDR} and width Γ_{GDR} for ^{16}O and $^{40,\,48}$Ca reproduce their corresponding experimental values $E_{\mathrm{GDR}}^{\mathrm{exp}}$ and $\Gamma_{\mathrm{GDR}}^{\mathrm{exp}}$. These chosen values of PDM parameters are then fixed in calculations for the neighbor neutron-rich isotopes ($N \geq Z$). The neutron pairing gap Δ_{n} is adjusted around the general trend $12/\sqrt{A}$ of the observed pairing gaps in stable nuclei to keep the GDR energy stable against varying the neutron number N.

Shown in Fig. 4 are the photoabsorption cross sections obtained within the PDM for ^{16,18,20,24}O. It is seen that the GDR becomes broader with increasing the neutron number N. Its width is particularly large for

^{18,20}O, for which the values of neutron pairing gap Δ_n are largest. This increase of GDR spreading enhances both of its low- and high-energy tails. In the region $E_\gamma \leq 15$ MeV, some weak structure of PDR is visible for ^{18,20}O, and also ^{22}O (not shown). In the rest of isotopes under study, except for an extension of the GDR tail toward lower-energy, there is no visible structure of the PDR.

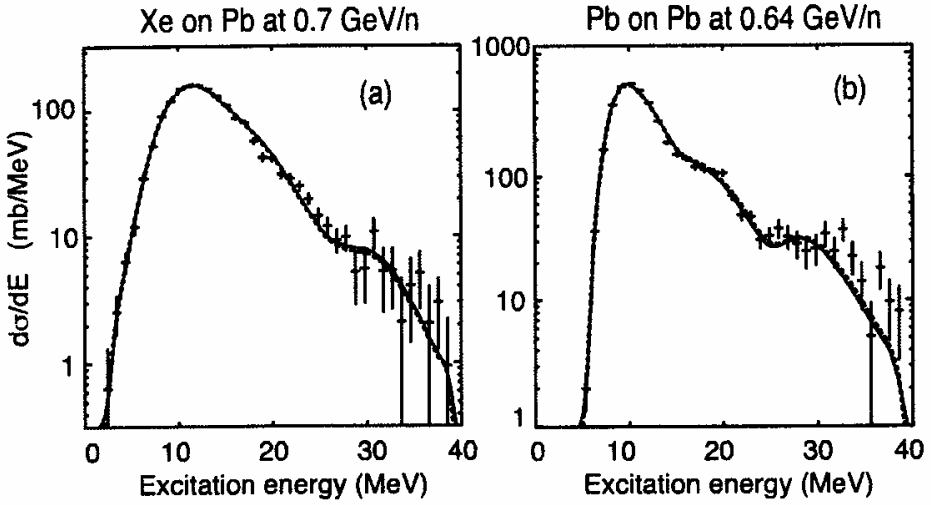

Fig, 3. Differential EM cross section for ^{136}Xe (*a*) and ^{208}Pb (*b*). Results obtained using EM cross section of DGDR within PDM (solid lines) and the best fit with χ^2 to the data points (dotted lines) are based on a normalization of GDR (the bump at ~ 10 MeV) which exhausts 90 % of TRK.

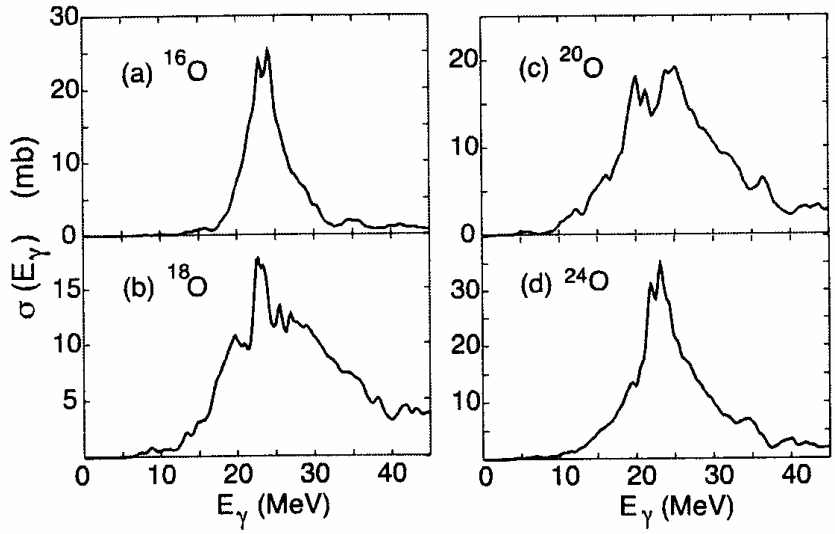

Fig. 4. Photoabsorption cross sections obtained within the PDM for some oxygen isotopes.

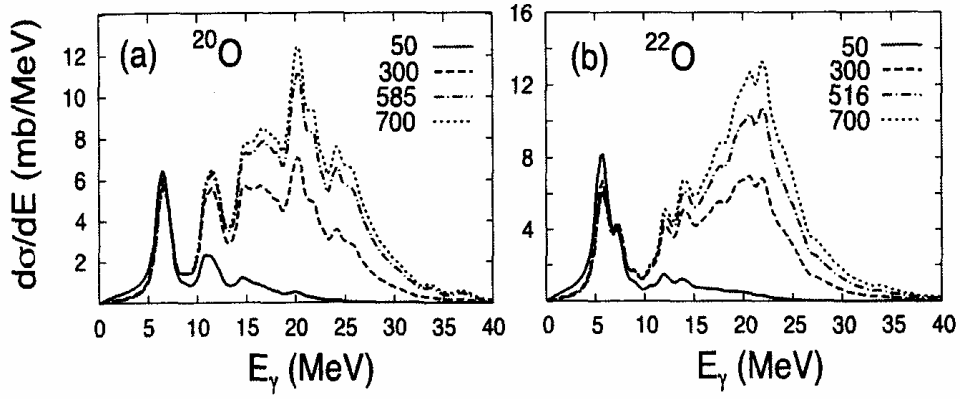

Fig. 5. Electromagnetic cross sections of GDR within PDM for ^{20,22}O on ^{208}Pb target.
Different lines display results obtained at different projectile energies as indicated in the panels.

Since the photon spectral function $N(E_\gamma)$ in the EM differential cross section $d\sigma_{\rm EM}/dE_\gamma$ (Eq. (17)) is an exponentially decreasing function with increasing E_γ, it enhances the low-energy part of the GDR. Therefore, the EM differential cross section $d\sigma_{\rm EM}/dE_\gamma$ of GDR can be used as a magnifying glass for the structure of PDR. These cross sections obtained within the PDM are shown in Fig. 5 for ^{20,22}O. The calculations were carried out for ^{208}Pb target at various projectile energies as shown in these figures. The PDR shows up in the EM cross sections as a well isolated peak located at around 6 MeV. Varying the projectile energy affects mostly the GDR region (above 10 MeV) of the EM cross section, but not the PDR.

4. Conclusions

A review is given on the current status of the study of nuclear resonances. It is demonstrated that the PDM is a simple but yet microscopic model, which is able to describe a variety of resonances under extreme conditions, namely: 1) the GDR at $T \neq 0$, including the constant width at T below 1 MeV, the width increase at low T, the width saturation at high T; 2) the EM cross sections for DGDR obtained at near-relativistic energy in ^{136}Xe and ^{208}Pb; 3) the possibility of extracting PDR in the EM cross sections of neutron-rich isotopes at low-energy beams.

Regarding the GDR at $T \neq 0$, it is shown that the mechanism of the width's increase at $1 \leq T \leq 3$ MeV and its saturation at $T > 3$ MeV comes from the coupling of the GDR to non-collective pp and hh configurations at $T \neq 0$. Meanwhile this effect is nearly cancelled by the monotonous decrease of the thermal pairing with increasing T at $T < 1$ MeV. As the result, the GDR width in this low T-region remains nearly temperature independent. This effect is confirmed by calculations in both of the PDM and a macroscopic approach, which takes into account thermal fluctuations of nuclear shapes and pairing field.

Concerning the DGDR, the PDM has succeeded to include the effect of anharmonicity between two coupled GDRs. As a result, for the first time, the experimental values of EM cross sections are nicely reproduced by theoretical calculations within the PDM for both ^{136}Xe and ^{208}Pb.

Finally, the results of calculations within the PDM have demonstrated how the pygmy dipole mode can be depleted due to its coupling to the GDR. This can be the case when the neutron excess cannot be well separated from the stable core. This effect leads to the disappearance of collectivity of the GDR. As a result the photoabsorption cross sections for neutron-rich isotopes have a tail extended toward low-energy region instead of a well-pronounced PDR peak. Nonetheless, since the photon spectral function $N(E_\gamma)$ in the EM differential cross is an exponentially decreasing function with increasing E_γ, it enhances the low-energy part of the E1-strength distribution, which is insensitive to the variation of beam energy. This feature suggests that a clean PDR peak (without admixture with the GDR) can be seen in the EM cross section (of neutron-rich oxygen and calcium isotopes, e.g.) using low-energy, but high-intensity beams at $\sim$ 50 MeV/n.

REFERENCES

1. *Harakeh M.N., van der Woude A.*, Giant resonances - Fundamental high-frequency modes of nuclear excitation. - Oxford: Clarendon Press, 2001. - 638 p.
2. *Schmidt R. et al.* // Phys. Rev. Lett. - 1993. - Vol. 70. - P. 1767; *Boretzky K. et al.* // Phys. Lett. - 1996. - Vol. B384. - P. 30; *Grünschloβ A. et al.* // Phys. Rev. - 1999. - Vol. C60. - P. 051601.
3. *Paar N. et al.* // Phys. Rev. - 2003. - Vol. 67. - P. 034312; *Sarchi D. et al.* // Phys. Lett. - 2004. - Vol. B601. - P. 27.
4. *Dinh Dang N., Arima A.* // Phys. Rev. Lett. - 1998. - Vol. 80. - P. 4145; Nucl. Phys. - 1998. - Vol. A636. - P. 427.
5. *Dinh Dang N. et al.* // Phys. Rev. - 2001. - Vol. C63. - P. 044302.
6. *Moretto L.G.* // Phys. Lett. - 1972. - Vol. B40. - P. 1.
7. *Dinh Dang N., Zelevinsky V.* // Phys. Rev. - 2001. - Vol. C64. - P. 064319; *Dinh Dang N., Arima A.* // Phys. Rev. - 2003. - Vol. C67. - P. 014304.
8. *Pshenichnov I.A. et al.* // Phys. Rev. - 1999. - Vol. C60. - P. 044901.
9. *Dinh Dang N. et al.* // Nucl. Phys. - 2000. Vol. A675. - P. 531.
10. *Bortignon P.F. et al.* // Nuc. Phys. - 1986. - Vol. A460. - P. 149; *Dinh Dang N.* // Nucl. Phys. - 1989. - Vol. A504. - P. 143.
11. *Kuznesov D. et al.* // Phys. Rev. Lett. - 1998. - Vol. 81. - P. 542.
12. *Arumugam P., Dinh Dang N.* // RIKEN Accel. Prog. Rep. - 2006. - Vol. 39. - P. 28.

ГИГАНТСКИЕ РЕЗОНАНСЫ ПРИ ЭКСТРЕМАЛЬНЫХ УСЛОВИЯХ

Н. Дин Данг

Представлено теоретическое описание гигантских резонансов при нулевой и конечной температурах. Исследованы следующие вопросы: 1) Гигантские дипольные резонансы (ГДР) в высоковозбужденных ядрах, включая области как низкой, так и высокой температуры. Результаты расчетов получены в рамках модели затухания фононов, модели тепловых флуктуаций формы, включающей тепловое спаривание. Результаты сравниваются с экспериментальными данными. 2) Электромагнитные сечения двойных ГДР (ДГДР) для ^{136}Xe и ^{208}Pb. Результаты, полученные в теоретических расчетах, сравниваются с экспериментальными данными для сечений ДГДР в эксклюзивных измерениях при околорелятивистских энергиях. 3) ГДР и дипольные пигми-резонансы (ДПР) в нейтронно-избыточных ядрах, для которых проанализирован эффект связи ГДР со сложными конфигурациями ДПР.

ГІГАНТСЬКІ РЕЗОНАНСИ ЗА ЕКСТРЕМАЛЬНИХ УМОВ

Н. Дін Данг

Представлено теоретичний опис гігантських резонансів при нульовій і кінцевій температурах. Досліджено такі питання: 1) Гігантські дипольні резонанси (ГДР) у високозбуджених ядрах, включаючи області як низької, так і високої температури. Результати розрахунків отримано в рамках моделі загасання фононів, моделі теплових флуктуацій форми, що включає теплове спарювання. Результати порівнюються з експериментальними даними. 2) Електромагнітні перетини подвійних ГДР (ПГДР) для ^{136}Xe і ^{208}Pb. Результати, отримані в теоретичних розрахунках, порівнюються з експериментальними даними для перетинів ПГДР в ексклюзивних вимірах при біляреляти вістських енергіях. 3) ГДР і дипольні пігмі-резонанси (ДПР) у нейтронно-надлишкових ядрах, для яких проаналізовано ефект зв’язку ГДР зі складними конфігураціями ДПР.